VNU Journal of Science: Mathematics - Physics

Journal homepage: https://js.vnu.edu.vn/MaP

Original Article

Construction of Sn_3O_4/g-C_3N_4 Composite with Enhanced Photocatalytic Activities Under Visible Light Irradiation

Vu Hoang Huong*

VNU University of Science, Vietnam National University, Hanoi,
334 Nguyen Trai, Thanh Xuan, Hanoi, Vietnam

Received 08 July 2022
Revised 23 September 2022; Accepted 06 October 2022

Abstract: The Sn_3O_4/g-C_3N_4 composites were produced by an annealing mixture of g-C_3N_4 and Sn_3O_4, which were prepared by calcining urea and hydrothermally treating of $SnCl_2$ solution, respectively. Chacterization of the samples was investigated by powder X-ray diffraction (XRD), Scanning electron microscope (SEM), Fourier transform infrared spectroscopy (FTIR), Photoluminescence (PL) and UV-Vis spectra. Studying the degradation of Rhodamine B (RhB) in the presence of visible light showed that the combination of Sn_3O_4 and g-C_3N_4 has an enhanced ability in the photocatalysis in comparison with the individual components. From kinetic investigations of RhB degradation, it is found that the SCN25 catalyst has the highest rate constant of 18.14 (min^{-1} x 10^3), which was about 11.4 times larger than that of pure g-C_3N_4. It is possible to explain the improved photocatalytic activity of Sn_3O_4/g-C_3N_4 composites by using the Z-scheme pathway.

Keyword: Visible light, Rhodamine B, Composite, Z-scheme.

1. Introduction

In recent years, the technology for photocatalytic degradation has grown quickly to clean the air and treat polluted water, which shows that it has a lot of potential uses. As a novel semiconductor photocatalytic material with a low band gap of 2.7 eV, graphite phase carbon nitride (g-C_3N_4) has been studied, focusing to the photocatalytic area of pollutant degradation [1]. The most major impediment to the practical deployment of g-C_3N_4 is a large recombination rate of charge carriers, resulting in lowering

* Corresponding author.
E-mail address: huongvh@hus.edu.vn

https//doi.org/10.25073/2588-1124/vnumap.4761

the efficency of the photocatalytic performance. The photocatalytic activity of g-C_3N_4 has been enhanced by numerous methods, including element doping, noble metal loading or heterostructure creation [2]. Researches showed that combining two semiconductors to form Z-scheme heterostructures is one of the most effective methods for decreasing charge carrier recombination. For example, the heterostructure is built by combining TiO_2 and g-C_3N_4 nanosheets as effective charge carrier collectors, which boosts photocatalytic effectiveness for removing RhB dye substantially [3]. However, the production of a heterostructure necessitates that two semiconductors have corresponding energy band potential positions and be in close proximity in order to permit the transfer and shuttle of charge carriers between them [4]. Researchers have identified an intermediate-valence molecule, multivalent tin oxides (for example, the multivalent tin oxides of Sn_3O_4, Sn_2O_3, Sn_5O_6), which shows some extremely fascinating physical and chemical properties due to the presence of oxygen vacancy [5]. According to theoretical and experimental studies, Sn_3O_4 is an excellent photocatalyst that may be used as a material to build heterostructures with other photocatalysts in order to enhance their photocatalytic activity [6].

As a result, in this work, Sn_3O_4/g-C_3N_4 composite heterostructures are created by a straightforward calcination method. The modification of Sn_3O_4 on g-C_3N_4 nanosheets increases the photocatalytic performance of g-C_3N_4 and expanding the use of multivalent tin oxide Sn_3O_4 in photocatalytic materials.

2. Experimental

2.1. Preparation and Characterizations

Thermal urea was used to produce g-C_3N_4. A particular quantity of urea was placed in a crucible, which was heated from room temperature to 550 °C at a rate of 2 °C/min and held for 4 h. After naturally cooling to ambient temperature, the yellow substance was collected and ground into a powder using an agate mortar.

Sn_3O_4 was prepared as follows. A certain percentage of $SnCl_2{\cdot}2H_2O$ and $Na_3C_6H_5O_7{\cdot}2H_2O$ were stirred until fully dissolved in distilled water. Then, a 5M NaOH solution was added and stirred until homogeneous. The solution was put into 100 mL autoclaves made of teflon and heated in an oven at 180 °C for 12 h. The generated yellow precipitates were washed many times with deionized water and ethanol, then dried in an oven at 60 °C for 12 h.

Here is a breakdown of the steps involved in making Sn_3O_4/g-C_3N_4 composite: g-C_3N_4 dissolved in distilled water was ultrasonically treated for 30 min, then a specified quantity of Sn_3O_4 was added to continue ultrasonic treatment for another 10 min, and then put in an oven at 250 °C for 2 h. It was possible to create composites with mass load ratios of 15%, 25%, and 35% by varying the Sn_3O_4 content. These heterostructures were designated as SCN15, SCN25 and SCN35.

A PANalytical Empyrean diffractometer was used to record the powder X-ray diffraction (XRD) patterns of the samples. The morphology of materials was examined using a Hitachi TM4000 scanning electron microscope (SEM). The FT-IR spectra were obtained using a Jasco 6300 spectrometer using KBr as the dispersion medium. The light absorption in the 200-800 nm wavelength range was studied using a UV-Visible/NIR Spectrophotometer UH4150. The PL spectra were collected using the Horiba JobinYvon Spex FL3-22 Fluorolog luminescence spectrometer.

2.2. Photocatalytic Activity Experiments

Experiments on photocatalytic activity were carried out using a 250 W Osram lamp with a 420 nm cut-off filter. The photocatalytic degradation activity of Sn_3O_4/g-C_3N_4 composite was evaluated using RhB as the target molecules. The experiment for photocatalytic degradation was carried-out as follows.

Under continual stirring, 25 mg of photocatalyst was disseminated in 100 mL RhB solution (10 mg/L). After a 10-minute ultrasonic treatment, the RhB solution was agitated in the dark for 30 min before illumination to achieve adsorption-desorption equilibrium between RhB and photocatalyst. At a predetermined time period (30 min), a 5 ml sample was obtained and centrifuged twice to remove sediment. An UV-vis spectrophotometer (Jasco, V-750) was used to measure the concentration of supernatant at 540 nm, which is the typical absorption wavelength of RhB.

3. Results and Discussion

The crystal structures and phase composition of g-C_3N_4, Sn_3O_4 and SCN25 were analyzed on XRD diffractometer, the obtained XRD patterns are shown in Fig. 1a. The XRD patterns of g-C_3N_4 exhibit two peaks at 2θ = 13.1 and 27.6°, which correspond to (002) planes of interlayer stacking of aromatic segments and (001) plane of triazine units (JSCPD 87-1256), respectively [7]. For pure Sn_3O_4, all the main diffraction peaks are located at 23.93°, 26.93°, 31.52°, 32.23°, 32.67°, 36.91°, 40.10°, 49.9°, 51.57°, 60.67°, 62.23° that conform to the typical patterns of the structure (JCPDS No.16-0737), corresponding to (101), (111), (-210), (-121), (210), (130), (102), (-301), (-1-32), (042), (312) lattice planes of Sn_3O_4, respectively [6]. The XRD patterns of the SCN25 composite material show a combination of Sn_3O_4 and g-C_3N_4 diffraction data, confirming successful preparation of the g-C_3N_4/Sn_3O_4 composites. No impurity diffraction peaks in Sn_3O_4, g-C_3N_4 and SCN25 are observed. This indicates that all the samples were formed in the single phase without impurities.

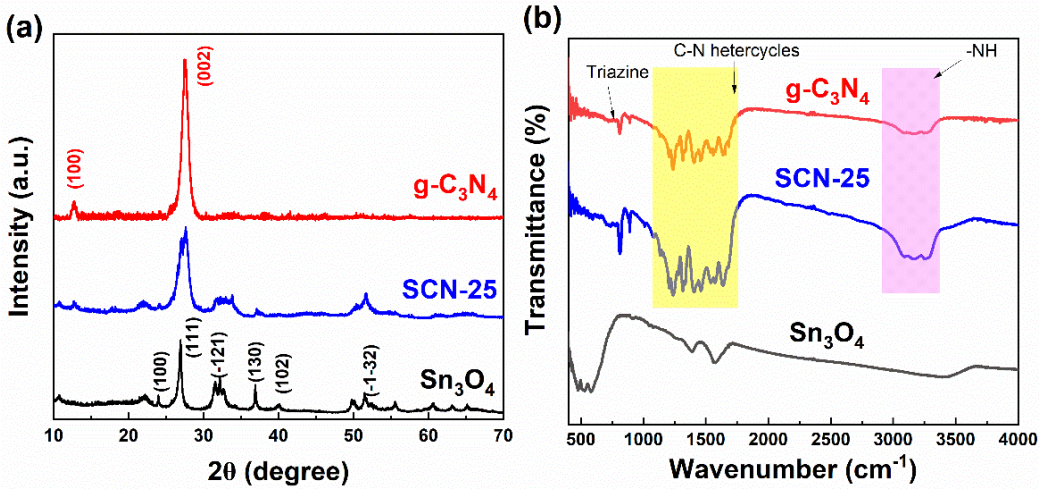

Figure 1. (a) XRD patterns; (b) FT-IR spectra of of g-C_3N_4, Sn_3O_4 and SCN25.

The bonding properties and the functional groups of samples were analyzed by using FT-IR spectra as shown in Fig. 1b. As to g-C_3N_4, the peak at 807 cm^{-1} corresponds to the vibration absorption of the s-triazine ring mode [8]. The set of peaks between 1140 cm^{-1} to 1740 cm^{-1} correspond to the stretching vibration modes of aromatic C-N heterocycles structural units [9]. The extensive absorption peaks between 3000 cm^{-1} and 3400 cm^{-1} are attributed to the C-N stretching and -NH groups [10]. Moreover, for Sn_3O_4, a weak peak around 531 cm^{-1} and 590 cm^{-1} observed in the FT-IR spectrum is ascribed to Sn-O stretching mode [8]. A broad absorption band near 3380 $cm^{-1}$is attributed to the O-H stretching vibrations of surface-adsorbed water, and 1628 cm^{-1} is H-O-H bending vibration of free water. In addition, the FTIR spectra provide additional evidence that the fundamental chemical structure of the

g-C_3N_4 is preserved in the SCN25. The bands at 1140 cm^{-1} and 1740 cm^{-1} were red-shifted in SCN25 composites, which can be explained due tothe interactions between Sn_3O_4 and g-C_3N_4.

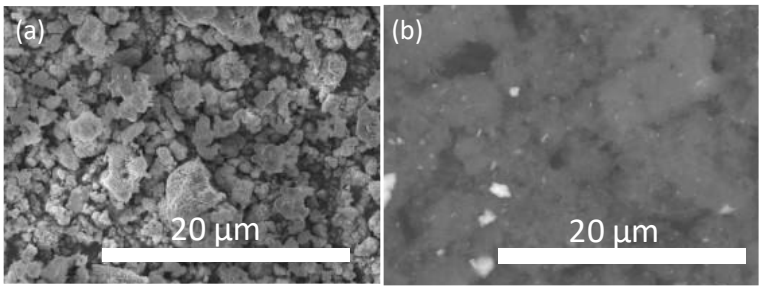

Figure 2. SEM images of (a) Sn_3O_4 and (b) SCN25.

A SEM image of Sn_3O_4 is shown in Fig. 2a, which shows a variety of hierarchical flower-like microstructures with a diameter of around 2.0 - 6.0 µm. Fig. 2b is the SEM image of SCN25. As can be seen, the g-C_3N_4 nanosheet has Sn_3O_4 bonded to its surface, showing that these two materials have been successfully combined.

After synthesizing Sn_3O_4 on g-C_3N_4, the optical absorption properties of the as-prepared materials are evaluated by UV–vis absorption spectra (Fig. 3a).

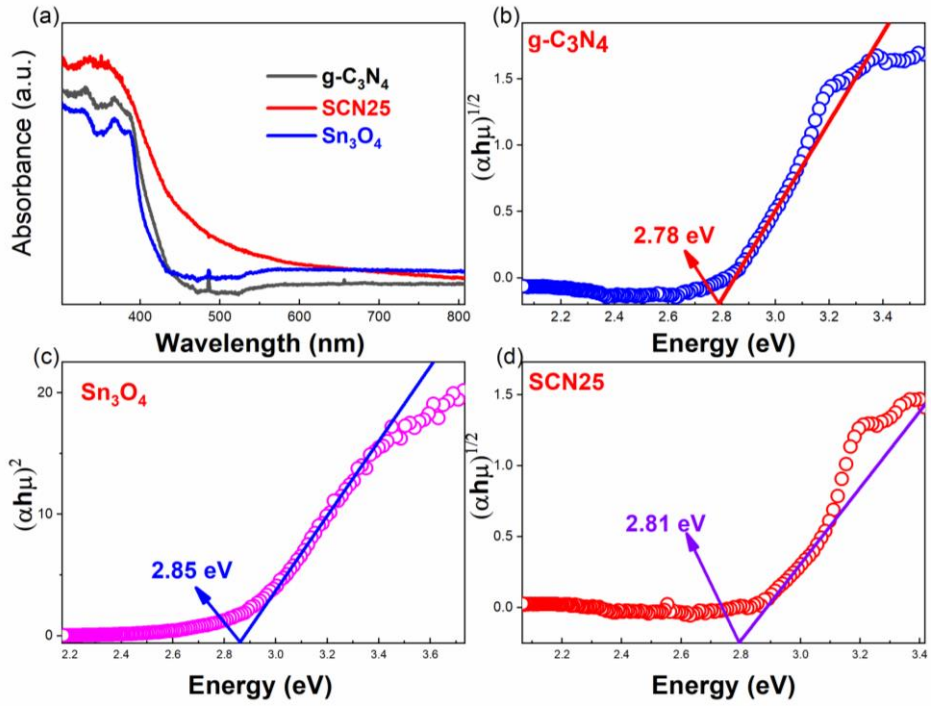

Figure 3. (a) UV-vis absorption spectra; (b, c, d) plots of $(\alpha hv)^n$ versus hv of g-C_3N_4, Sn_3O_4 and SCN25.

Observations reveal that the samples display a strong absorption in the wavelength region of 300 – 500 nm. Compared to g-C_3N_4, the SCN25 composite shows a noticeable red-shift in the absorption edge, which may be due to the influence of Sn_3O_4 on the surface of g-C_3N_4 nanosheets. It means that the strong

contact between Sn_3O_4 and g-C_3N_4 is generated, which is helpful for improving charge carrier separation efficiency and heterostructure stability. According to Tauc's plot, the band gap energies (E_g) of the g-C_3N_4, Sn_3O_4 and SCN25 composites may be calculated from following formula:

$$(\alpha h\upsilon) = A(h\upsilon - Eg)^{n/2}$$

where α is the absorbance, h is the Planck constant and υ is light frequency, respectively [4]. As illustrated in Figs. 3 (b, c, d), the Eg of g-C_3N_4, Sn_3O_4 and SCN25 are determined to be 2.78, 2.85 and 2.81 eV, respectively. With the coupling effect of Sn_3O_4 narrowing the band gap in g-C_3N_4, the SCN25 heterostructure seems to be more amenable to visible light excitation, which might improve photocatalysis efficiency.

3.1. Photocatalytic Degradation Activity

The degradation of RhB under visible light irradiation is used to test the photocatalytic activity of freshly produced materials. The degradation dynamic curves of RhB over the g-C_3N_4, Sn_3O_4, and SCN heterostructures are shown in Fig. 4a. Within 150 min, the g-C_3N_4 and Sn_3O_4 degradation rates are only 24 percent and 8 percent, respectively. In contrast, when Sn_3O_4 are changed on the surface of g-C_3N_4 nanosheets by increasing Sn_3O_4 concentration, RhB degradation rates over Sn_3O_4/g-C_3N_4 heterostructures likewise rise dramatically. The degradation rate of RhB reaches a maximum of 98.4% within 150 min when the concentration of Sn_3O_4 is 25 weight percent, which is about three times that of g-C_3N_4 (24%). Nonetheless, as the amount of Sn_3O_4 increases, the rate of degradation begins to decrease. This may be due to the shielding effect reducing the light harvesting capability of g-C_3N_4 and the formation of recombination centers reducing the separation efficiency of electron-hole pairs originating from excess Sn_3O_4 on the surface of g-C_3N_4 [4]. In order to provide a precise quantitative comparison, the kinetic equation of a first-order process is utilized to describe the photocatalytic degradation of RhB. The rate constants are calculated by fitting the data to the equation $\ln(C_0/C) = kt$ (Fig. 4b) [11].

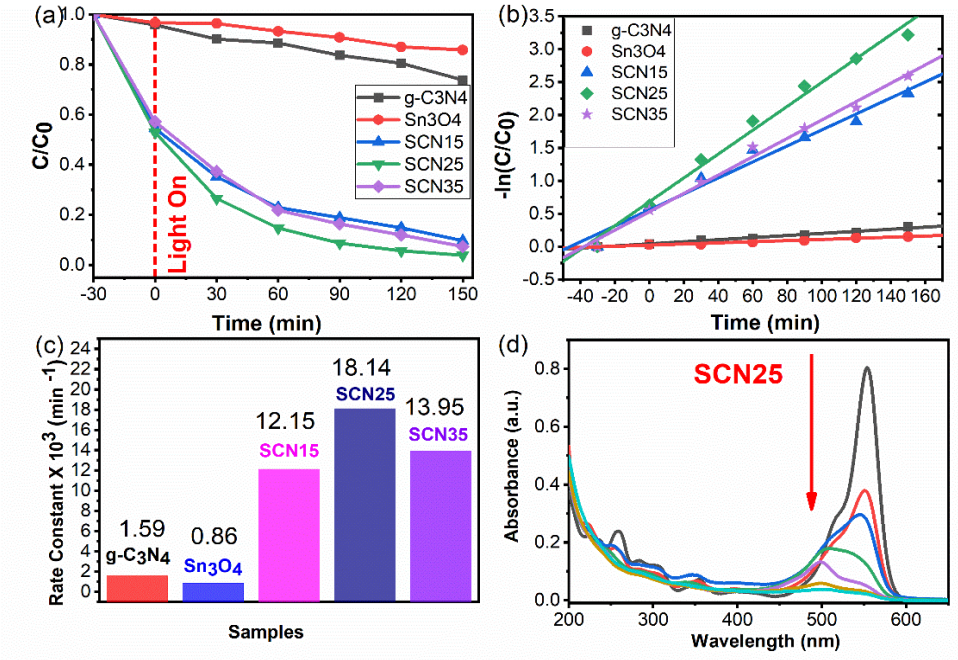

Figure 4. (a) Degradation dynamic curves, (b) plots of $\ln(C_0/C)$ versus time, (c) rate constants of RhB over different samples, and absorbance of RhB over SCN25 composite (d).

As seen in Fig. 4c, the greatest rate constant k value of SCN25 heterostructure is 18.14 ($min^{-1} \times 10^3$), which is about four times larger than that of g-C_3N_4 (1.59 $min^{-1} \times 10^3$). Fig. 4d demonstrates the absorbance fluctuation of RhB solution over SCN25 heterostructure throughout the photocatalytic degradation process. The absorbance of RhB solutions reduces significantly across the whole range of 200-650 nm as a result of the degradation process, indicating that the ring structures have been damaged and degraded into tiny organic/inorganic molecules.

It is known that the fluorescence emission from photocatalyst charge carriers has a strong correlation with the charge carrier separation and transit efficiency of samples [11]. By comparing PL emission spectra in Fig. 5, the SCN25 composite exhibits reduced fluorescence intensity compared to g-C_3N_4, indicating that the effective interfacial charge transfer between g-C_3N_4 and Sn_3O_4 inhibits electron-hole pair recombination. On the basis of the aforementioned experimental findings, we suggest the photocatalytic reaction mechanism of RhB over SCN25 composite as shown in Fig. 5. Therefore, when g-C_3N_4 and Sn_3O_4 produce composite materials, a Z-scheme heterostructure should be created between them. Under the influence of visible light, the electrons on the valence band (VB) of g-C_3N_4 and Sn_3O_4 will move to the conduction band (CB), accompanied by the formation of holes on their respective (VB). Then, the electrons on CB of Sn_3O_4 and the holes on VB of g-C_3N_4 rapidly recombine at their contact. Simultaneously, the excess electrons on CB of g-C_3N_4 and the holes on VB of Sn_3O_4 move to their respective surfaces. The effectiveness of charge carrier separation may be improved greatly by transferring charge between Sn_3O_4 and g-C_3N_4. Afterwards, O_2 dissolved in water can be adsorbed on the surface of g-C_3N_4 and react with electrons to form $\bullet O_2^-$. In the meanwhile, the surface of Sn_3O_4 may also oxidize OH^- to form •OH. Finally, the superoxide free radical $\bullet O_2^-$ and •OH will oxidize RhB molecules directly

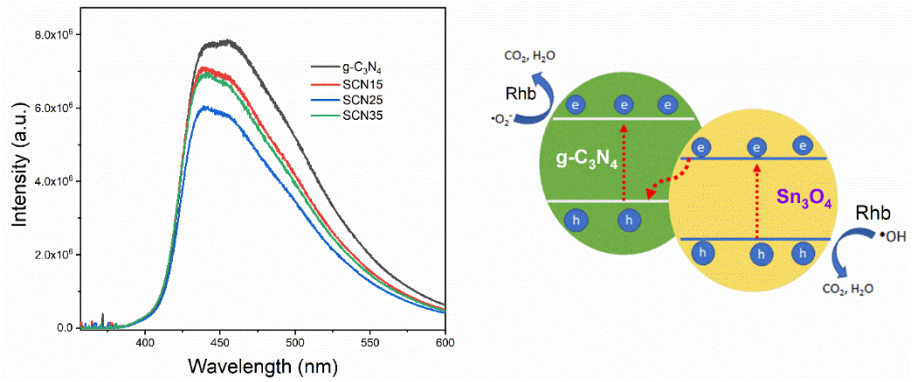

Figure 5. Photocatalytic reaction mechanism of RhB over SCN25 under the visible light irradiation.

4. Conclusion

In summary, we have described the fabrication of a Sn_3O_4/g-C_3N_4 composite by modifying Sn_3O_4 hierarchical flower-like microstructures on the surface of g-C_3N_4 nanosheets. It demonstrated the best photocatalytic activity for eliminating RhB when the load of Sn_3O_4 is of 25 wt.%, with a degradation rate and rate constant within 150 min that are up to 4 and 11.4 times more than g-C_3N_4, respectively. Charge carrier recombination is greatly reduced, and charge carrier separation is enhanced as a result of Sn_3O_4 and g-C_3N_4 being combined to form a composite. g-C_3N_4 photocatalytic efficiency can be improved by generating a Z-scheme heterostructure.

Acknowledgements

This research is funded by Asia Research Center (ARC) under grant CA.21.5A. The author also thanks Dr. Nguyen Van Can (Department of Chemical Engineering, National Cheng Kung University, Taiwan) for his equipment supports.

References

[1] J. Singh, P. Kumari, S. Basu, Degradation of Toxic Industrial Dyes Using SnO_2/g- C_3N_4 Nanocomposites: Role of Mass Ratio on Photocatalytic Activity, Journal of Photochemistry and Photobiology A: Chemistry, Vol. 371 , 2019, pp. 136-143, https://doi.org/10.1016/j.jphotochem.2018.11.014.

[2] J. Liang, X. Yang, Y. Wang, P. He, H. Fu, Y. Zhao, Q. Zou, X. An, A Review on g-C_3N_4 Incorporated with Organics for Enhanced Photocatalytic Water Splitting, Journal of Materials Chemistry A, Vol. 9, No. 22, 2021, pp. 12898-12922, https://doi.org/10.1039/D1TA00890K.

[3] Z. Tong, D. Yang, T. Xiao, Y. Tian, Z. Jiang, Biomimetic Fabrication of g-C_3N_4/TiO_2 Nanosheets with Enhanced Photocatalytic Activity Toward Organic Pollutant Degradation, Chemical Engineering Journal, Vol. 260, 2015, pp 117-125, https://doi.org/10.1016/j.cej.2014.08.072.

[4] C. Li, S. Yu, H. Dong, C. Liu, H. Wu, H. Che, G. Chen, Z-scheme Mesoporous Photocatalyst Constructed by Modification of Sn_3O_4 Nanoclusters on g-C_3N_4 Nanosheets with Improved Photocatalytic Performance and Mechanism Insight, Applied Catalysis B: Environmental, Vol. 238, 2018, pp. 284-293, https://doi.org/10.1016/j.apcatb.2018.07.049.

[5] Y. He, D. Li, J. Chen, Y. Shao, J. Xian, X. Zheng, P. Wang, Sn_3O_4: A Novel Heterovalent-Tin Photocatalyst with Hierarchical 3D Nanostructures Under Visible Light, RSC Advances, Vol. 4, 2014, pp. 1266-1269, https://doi.org/10.1039/C3RA45743E.

[6] Y. S. Liu, A. Yamaguchi, Y. Yang, H. Abe, S. Ueda, T. Tanabe, M. Miyauchi, Visible-Light-Induced CO_2 Reduction by Mixed-Valence Tin Oxide, ACS Applied Energy Materials, Vol. 4, 2021, pp. 13415-13419, https://doi.org/10.1021/acsaem.1c02896.

[7] W. Lei, F. Wang, X. Pan, Z. Ye, B. Lu, Z-scheme MoO_3-2D SnS Nanosheets Heterojunction Assisted g-C_3N_4 Composite for Enhanced Photocatalytic Hydrogen Evolutions, International Journal of Hydrogen Energy, Vol. 47, 2022, pp. 10877-10890, https://doi.org/10.1016/j.ijhydene.2022.01.139.

[8] L. Yang, J. Huang, L. Shi, L. Cao, H. Liu, Y. Liu, Y. Li, H. Song, Y. Jie, J. Ye, Sb Doped SnO_2-Decorated Porous g-C_3N_4 Nanosheet Heterostructures with Enhanced Photocatalytic Activities Under Visible Light Irradiation, Applied Catalysis B: Environmental, Vol. 221, 2018, pp. 670-680, https://doi.org/10.1016/j.apcatb.2017.09.041.

[9] H. Wu, S. Yu, Y. Wang, J. Han, L. Wang, N. Song, H. Dong, C. Li, A Facile One-Step Strategy to Construct 0D/2D SnO_2/g-C_3N_4 Heterojunction Photocatalyst for High-Efficiency Hydrogen Production Performance from Water Splitting, International Journal of Hydrogen Energy, Vol. 45, 2020, pp. 30142-30152, https://doi.org/10.1016/j.ijhydene.2020.08.112.

[10] M. Ismael, E. Elhaddad, M. Wark, Construction of SnO_2/g-C_3N_4 Composite Photocatalyst with Enhanced Interfacial Charge Separation and High Efficiency for Hydrogen Production and Rhodamine B Degradation, Colloids and Surfaces A: Physicochemical and Engineering Aspects, Vol. 638, 2022, pp. 128-288, https://doi.org/10.1016/j.colsurfa.2022.128288.

[11] D. P. Bui, T. D. Nguyen, T. T. L. Vo, T. M. Cao, S. J. You, V. V. Pham, SnO_2–x Nanoparticles Decorated on Graphitic Carbon Nitride as S-Scheme Photocatalysts for Activation of Peroxymonosulfate, ACS Applied Nano Materials, Vol. 4, 2021, pp. 9333-9343, https://doi.org/10.1021/acsanm.1c01801.